JOURNAL OF MATERIALS SCIENCE 17 (1982) 3361–3370

A $\Sigma=27$ coincidence grain boundary in a Cu–Ni alloy

TH. KARAKOSTAS, G. L. BLERIS
Physics Department, University of Thessaloniki, Greece

J. G. ANTONOPOULOS
Department of Electrical Engineering, Demokritus University of Thrace, Xanthi, Greece

P. DELAVIGNETTE
Materials Science Department, SCK/CEN, B-2400 Mol, Belgium

A systematic method has been used to characterize a particular grain boundary in a Cu–Ni alloy. Its multiplicity is $\Sigma = 27a$ and a deviation from that orientation has been calculated and expressed by a small-angle rotation matrix. The deviation angle of 50′ has been calculated by electron diffraction patterns and also on the basis of the intrinsic dislocation structure. These have been found to be of the same type as the matrix dislocations, having also a relation to the $\Sigma = 27a$ orientation relationship.

1. Introduction

Different models have been proposed for the analysis of the structure of grain boundaries. The most frequently used is based on the concept of coincidence site lattice (CSL) [1]. The plane matching (PM) model gives also a good explanation of the problem [2]. Closely related to the latter, the concept of the coincidence axis direction (CAD) [3] is also proposed. A detailed review of these models has recently been published [4]. The identification of an observed grain boundary with one of these models is only possible if the relevant parameters are experimentally determined with a high degree of accuracy.

The identification of a particular grain boundary with a CSL is achieved by comparison of its orientation relationship with those of tabulated CSL models. Of course, any bicrystal orientation relationship characterizing a grain boundary may be associated to a CSL relationship if a high enough multiplicity Σ [1] and a certain deviation is accepted. Therefore, the maximum value of Σ which is physically meaningful should be defined, and this is clearly not achieved so far.

In a series of papers [5–12], a method for the characterization of a bicrystal has been developed, the main principles of which are the following. First, the orientation of each crystal element of a grain boundary is determined in TEM by electron diffraction patterns, using an experimental co-ordinate system. Possible values of Σ within a predetermined approximation are found, in comparison with pre-established tables of theoretical rotation operations characterizing CSLs up to $\Sigma < 100$. Then, all equivalent rotation axes describing this bicrystal are calculated using the experimental co-ordinate system. This allows these values to be tested experimentally. In particular, such a rotation axis, adjusted parallel to the electron beam, allows an observation of identical diffraction patterns for both crystal elements, rotated by a known rotation angle.

In this paper a grain boundary in a Cu–Ni alloy has been studied in detail using this method. The multiplicity has been determined to be $\Sigma = 27a$. A diffraction analysis was carried out and its results are in complete and perfect agreement with the predicted CSL model. Taking into account the accuracy of this determination, this example gives strong evidence that the existence of a grain boundary with a relatively large multiplicity has been effectively established.

0022–2461/82/113361–10$03.70/0

2. Characterization of the grain boundary

Long-annealed (168 h at 900° C) Cu–Ni specimens have been electropolished for TEM observation. A particular grain boundary showing a set of nearly parallel and equidistant dislocations, visible in dark-field images (Fig. 1), has been selected. It is clear that these dislocations are closely related to the structure of the grain boundary, and that they reveal the presence of a structural continuity along the boundary for which an interpretation in terms of CSL will be proposed.

From the experimental co-ordinates α, δ and the relevant diffraction patterns for both crystal elements [5], the 24 equivalent descriptions (rotation axes and rotation angles) characterizing this grain boundary have been calculated using the program GB1 [12]. These are listed in Table I, together with their instrumental co-ordinates α, δ, and illustrated on a stereographic projection in Appendix 1. Using the u, v, w values of the closest to 180° rotation description and the stereographic projection giving all the CSLs up to $\Sigma < 50$ [8] this grain boundary may be described within a high accuracy as $\Sigma = 27a$ (180° rotation along [511]), as is indicated in Fig. 2. In a further step, the small-angle rotation matrix, R^i, is calculated [8]. It characterizes the deviation of an experimental bicrystal rotation relationship from a tabulated model (rotation angle for $R^t = 180°$), according to the relation:

$$R^i = R^e \cdot R^t, \tag{1}$$

where the rotation matrix

$$R^e = \begin{bmatrix} 0.8452 & 0.3723 & 0.3834 \\ 0.3737 & -0.9246 & 0.0739 \\ 0.3820 & 0.0808 & -0.9206 \end{bmatrix}, \tag{2}$$

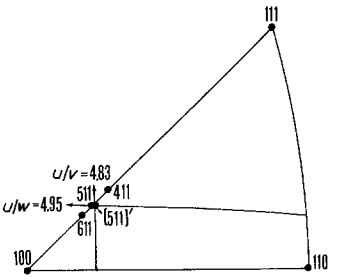

Figure 2 Stereographic projection showing the projection of $\Sigma = 9$ [411], $\Sigma = 19$ [611], $\Sigma = 27a$ [511] and the experimentally observed bicrystal [511]'.

is obtained from the program GB1 for the highest rotation angle given in Table I and the matrix

$$R^t = \frac{1}{27}\begin{bmatrix} 23 & 10 & 10 \\ 10 & -25 & 2 \\ 10 & 2 & -25 \end{bmatrix}, \tag{3}$$

describes a rotation of 180° around the [511] axis. The matrix R^t may be easily constructed using the expression for the 180° rotatation matrix [7] and taking into account that:

$$\alpha = \frac{5}{27^{1/2}}, \quad \beta = \frac{1}{27^{1/2}}, \quad \gamma = \frac{1}{27^{1/2}}. \tag{4}$$

Thus, the matrix R^i has the form:

$$R^i = \begin{bmatrix} 0.9999 & -0.0033 & -0.0144 \\ 0.0033 & 1.0000 & 0.0015 \\ 0.0144 & -0.0015 & 0.9999 \end{bmatrix}, \tag{5}$$

and describes a rotation of $\epsilon = 0.85° = 51'$ around the axis

$$[-0.10 \quad -0.97 \quad 0.22] \tag{6}$$

in crystal 2 co-ordinates.

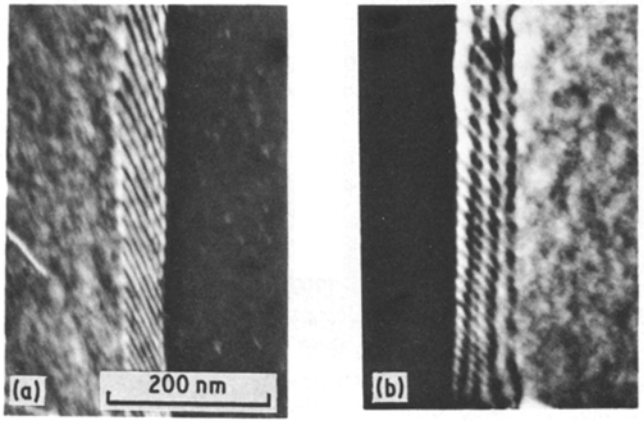

Figure 1 Dark-field images of grain-boundary dislocations taken with: (a) the $0\bar{2}2$ reflection of crystal 1, (b) the $11\bar{3}$ reflection of crystal 2.

TABLE I The 24 equivalent descriptions of the observed bicrystal in decreasing order of the rotation angle

Angle	u	v	w	α	δ
179.80	0.96	0.19	0.20	147.67	8.40
179.59	0.28	−0.68	−0.68	−117.28	43.77
164.37	0.54	0.14	0.83	103.79	−0.83
164.07	−0.83	−0.14	0.54	14.44	−30.20
163.95	0.83	−0.55	0.14	134.55	−63.00
163.66	0.55	0.83	0.14	120.36	59.94
157.61	−0.20	0.00	0.98	58.60	−6.72
157.02	0.20	−0.98	0.00	−98.06	85.51
147.70	−0.00	−0.71	0.71	74.03	−54.65
147.16	−0.50	−0.71	0.50	47.54	−74.51
146.95	0.50	−0.50	0.71	101.89	−40.06
123.04	0.32	0.77	0.55	98.93	42.27
122.81	0.77	−0.55	−0.32	−143.81	77.35
122.38	0.77	−0.33	−0.54	−153.62	47.13
122.15	0.32	0.55	0.77	93.93	24.60
114.86	0.16	−0.97	0.16	92.94	−86.37
114.37	−0.17	−0.17	0.97	60.38	−17.95
94.93	0.65	−0.38	0.66	11.82	−34.07
94.65	−0.66	−0.65	0.39	39.02	−85.34
94.64	0.93	0.38	0.01	152.41	38.34
94.24	0.93	−0.01	0.38	137.88	−11.82
70.53	−0.24	0.25	0.94	57.83	10.22
69.82	0.24	−0.94	−0.21	−105.32	73.07
32.30	−0.01	−0.75	0.70	74.06	−55.54

3. Further identification using diffraction patterns

The 24 equivalent descriptions for the model $\Sigma = 27a$ as tabulated in [10] are presented in Table II. These are compared with the experimental data given in Table I. It appears that a description exists with a $[0\bar{1}1]$ rotation axis. Therefore, the corresponding $0\bar{2}2$ reflection is common to both crystal elements. This is illustrated in Fig. 3. In Fig. 3a the pattern for crystal 1 appears to deviate slightly from a 111 pattern. Similarly, in Fig. 3b a pattern which is nearly 110 appears for crystal 2. Fig. 3c, showing clearly the common $[0\bar{1}1]$ rotation axis, is taken within a selected area including both crystal elements. If, on the other hand, this direction is adjusted parallel to the electron beam, two identical diffraction patterns rotated to each other by an angle of 31.57° should appear, according to Table II. This is illustrated in Fig. 4 showing the three diffraction patterns taken from crystal 1, from crystal 2 and from both crystal elements, respectively.

The 180° rotation axis [511] is also examined. Fig. 5a and b taken in each crystal element give, for both, a $\bar{1}14$ crystal orientation. The [511]

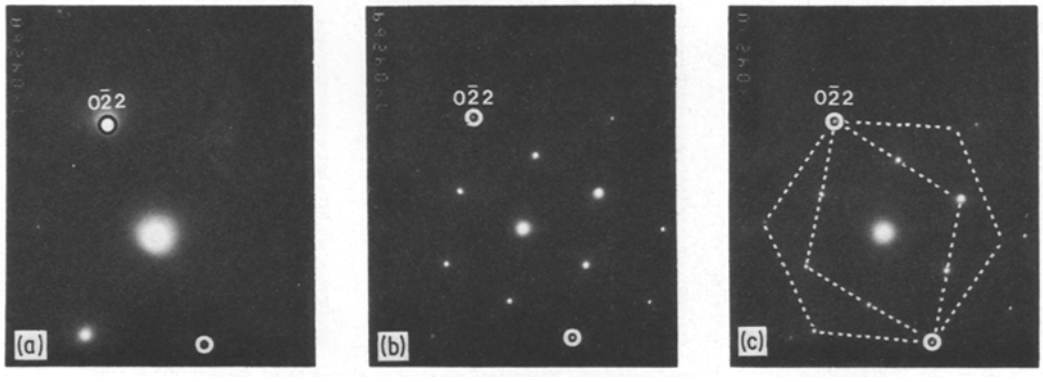

Figure 3 The common $0\bar{2}2$-type reflection (encircled) for the $\Sigma = 27a$ CSL bicrystal. The diffraction patterns are (a) from crystal 1, (b) from crystal 2 and (c) from both crystals.

TABLE II The symmetrically equivalent descriptions of the $\Sigma = 27a$ based on the 180° description [10]

Angle	$u\,v\,w$	Angle	$u\,v\,w$
180	5 1 1	122.48	$7\,\bar{3}\,\bar{5}$
	$\bar{2}\,5\,5$		$7\,\bar{5}\,\bar{3}$
164.35	$6\,1\,\bar{4}$		3 5 7
	4 6 1		3 7 5
	4 1 6	144.04	$\bar{1}\,\bar{1}\,6$
	$6\,\bar{4}\,1$		$1\,\bar{6}\,1$
157.81	$\bar{1}\,0\,5$	95.31	$5\,5\,\bar{3}$
	$1\,\bar{5}\,0$		$5\,\bar{3}\,5$
148.41	$0\,\bar{1}\,1$	94.25	5 0 2
146.44	$5\,\bar{5}\,7$		5 2 0
	$5\,7\,\bar{5}$	70.53	$\bar{1}\,1\,4$
			$\bar{1}\,4\,1$
		31.59	$0\,\bar{1}\,1$

180° rotation axis is shown in Fig. 5c which has been taken on both crystal elements. The rotation relationship of an angle of 70.53° for the $[\bar{1}14]$ axes is also clearly revealed.

It is remarkable to note that all these patterns have been obtained by setting the experimental orientation data on the value predicted by the calculations.

4. Small-angle rotation matrix

Finally, the small-angle rotation matrix of Equation 5 is examined. First, an application of the program GB3 will give all possible CSLs that are compatible with the experimentally observed grain boundary within a predetermined orientation approximation, taken in this case as 8°. The results for deviation angles smaller than this value and for Σ up to 99 are given in Table III. The characterization with $\Sigma = 27a$ is by far the best, therefore the other models given in Table III will not be considered further.

In order to calculate the deviation of the experimental rotation axis from its exact [511] position, which is the common rotation axis for both crystals, the vector field [dx] is used [8]:

$$[\mathrm{dx}] = [I - R^{\mathrm{t}}(R^{\mathrm{e}})^{-1}]\,[x]_2. \tag{7}$$

If the rotation angle for R^{t} is 180°, then:

$$R^{\mathrm{i}} = R^{\mathrm{e}} \cdot R^{\mathrm{t}} = I + R^{\mathrm{s}}, \tag{8}$$

where R^{s} is a skew symmetric matrix and

$$(R^{\mathrm{i}})^{-1} = R^{\mathrm{t}}(R^{\mathrm{e}})^{-1} = I - R^{\mathrm{s}}. \tag{9}$$

Therefore, Equation 7 becomes:

$$[\mathrm{dx}] = [I - I + R^{\mathrm{s}}]\,[x]_2 = R^{\mathrm{s}}\,[x]_2, \tag{10}$$

where:

$$R^{\mathrm{s}} = \begin{bmatrix} 0 & -0.0033 & -0.0144 \\ 0.0033 & 0 & 0.0015 \\ 0.0144 & -0.0015 & 0 \end{bmatrix}. \tag{11}$$

By taking, from Table I, the co-ordinates of the [511] experimental rotation axis, Equation 10 becomes:

$$[\mathrm{dx}] = R^{\mathrm{s}} \begin{bmatrix} 0.961 \\ 0.194 \\ 0.199 \end{bmatrix} = \begin{bmatrix} -0.0035 \\ 0.0035 \\ 0.0136 \end{bmatrix}. \tag{12}$$

The vector [dx] is illustrated in Fig. 6, where the angle $\Delta\varphi$ between the vectors $[\mathrm{x}] = [x_1, x_2, x_3]$ and $[\mathrm{x} + \mathrm{dx}] = [x_1 + \mathrm{d}x_1,\ x_2 + \mathrm{d}x_2,\ x_3 + \mathrm{d}x_3]$ may easily be determined from the relation:

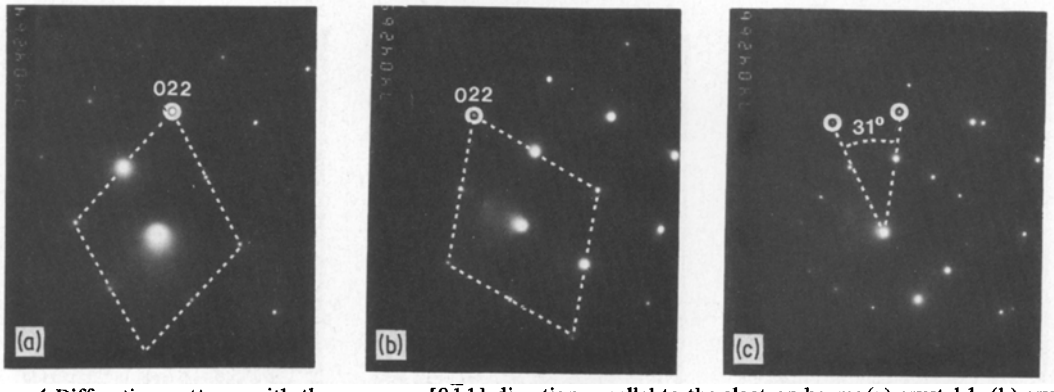

Figure 4 Diffraction patterns with the common $[0\bar{1}1]$ direction parallel to the electron beam; (a) crystal 1, (b) crystal 2, and (c) superposition of the two previous patterns, showing an approximate rotation angle of 31°, in agreement with Tables I and II.

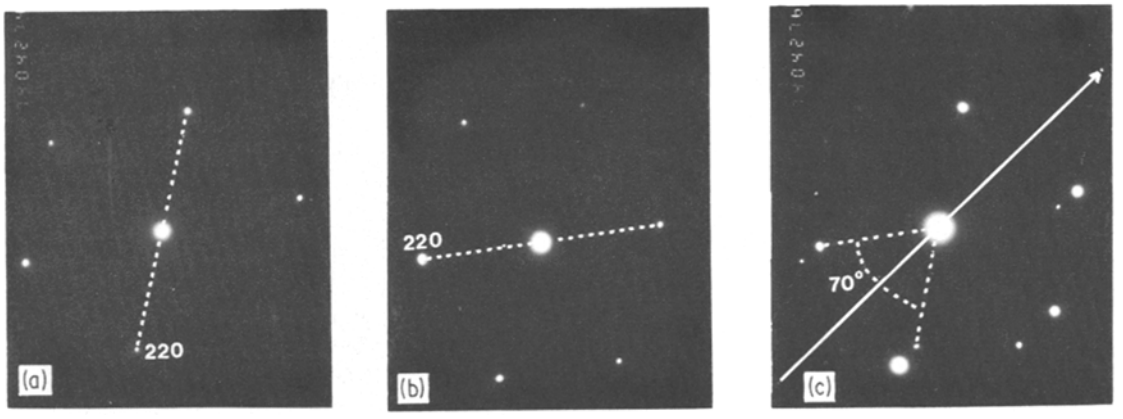

Figure 5 (a) Diffraction patterns from crystal 1, (b) diffraction pattern from crystal 2, and (c) the superposition of the two previous patterns. The 511 reflection showing the rotation axis of the 180° description is indiated by the arrow and the 70.53° around the [$\bar{1}$14] axis by the broken lines.

$$\Delta\varphi = 2 \arcsin \frac{||\mathbf{dx}||}{2}, \tag{13}$$

where $||\mathbf{dx}||$ is the measure of the vector [dx] of Equation 12. The calculation gives $\Delta\varphi = 0.83° = 50'$. This is also visible in Fig. 7 from the doubled 511 reflections. Precautions have been taken to ensure that these two reflections have the same intensity in order to minimize the projection errors. A measurement of the angle on the diffraction pattern gives a value of $\Delta\varphi = 0.82° = 49'$, in agreement with that calculated from Equation 13.

5. Boundary-plane characterization

The boundary plane is easily determined using the electron diffraction patterns when the boundary plane is in a vertical position. Diffraction patterns are presented in Fig. 8a for crystal 2 and in Fig. 8b for both crystal elements. In Fig. 8a the electron beam is nearly parallel to the [010] zone axis, while for crystal 1 it is near [1$\bar{3}$0] as illustrated in Fig. 8b together with its schematic extension, where the black dots represent the reflections of crystal 1 and the open circles the reflections of crystal 2. The direction perpendicular to the boundary plane is marked by a solid line. From this it can be deduced that the boundary plane is (104) for crystal 2 and near to (6 2 $\bar{8}$) for crystal 1.

This latter boundary plane may also be calculated using the theoretical and experimental rotation matrices from the relation:

$$x_1 = R^{-1} \cdot x_2. \tag{14}$$

This gives for the theoretical matrix:

$$(x_1)_{th} = \frac{1}{27} \begin{bmatrix} 23 & 10 & 10 \\ 10 & -25 & 2 \\ 10 & 2 & -25 \end{bmatrix} \begin{bmatrix} 1 \\ 0 \\ 4 \end{bmatrix} = \begin{bmatrix} 7 \\ 2 \\ -10 \end{bmatrix}, \tag{15}$$

and for the experimental matrix:

TABLE III Small-angle operations for $\Sigma < 100$ and $\Sigma < 8°$ according to 180° description

Σ	u	v	w	Small angle	x_1	x_2	x_3
9	4	1	1	6.46	−0.01	0.66	−0.75
19	6	1	1	5.78	−0.02	−0.76	0.65
27	5	1	1	0.85	−0.10	−0.97	0.22
61	8	7	3	7.16	−0.08	−0.23	0.97
67	11	3	2	7.37	0.27	−0.28	−0.92
77	9	8	3	7.62	0.27	−0.52	0.81
89	9	2	2	2.63	−0.03	0.58	−0.82
91	13	3	2	6.67	0.24	−0.86	−0.46

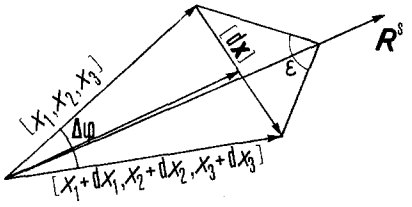

Figure 6 Geometrical representation for the calculation of the angle ϵ.

$$(x_1)_{exp} = \begin{bmatrix} 0.8452 & 0.3723 & 0.3834 \\ 0.3737 & -0.9246 & 0.0739 \\ 0.3820 & 0.0808 & -0.9200 \end{bmatrix} \begin{bmatrix} 1 \\ 0 \\ 4 \end{bmatrix}$$

$$\approx \begin{bmatrix} 7.108 \\ 2 \\ -9.865 \end{bmatrix}. \qquad (16)$$

Equation 16 indicates, in a good approximation with the results of Equation 15, the $(72\bar{1}0)$ plane for crystal 1 and is in agreement with the experimental value deduced from Fig. 8b. This shows that the boundary plane is *not* of the same crystallographic type for both crystal elements.

6. Burger's vector determination

Using contrast experiments it has been possible to reveal only one set of dislocations. These are visible in Fig. 9. Reflections of crystal 1 (a to d) and reflections of crystal 2 (e to h) have been used. The dislocations run along the $[\bar{4}11]$ direction for crystal 2, which corresponds to the [877] direction for crystal 1, as deduced from Equation 14. By applying the invisibility criterion, $\mathbf{g} \cdot \boldsymbol{b} = 0$, on the micrographs of Fig. 10, their Burger's vector has been determined. In Fig. 10a

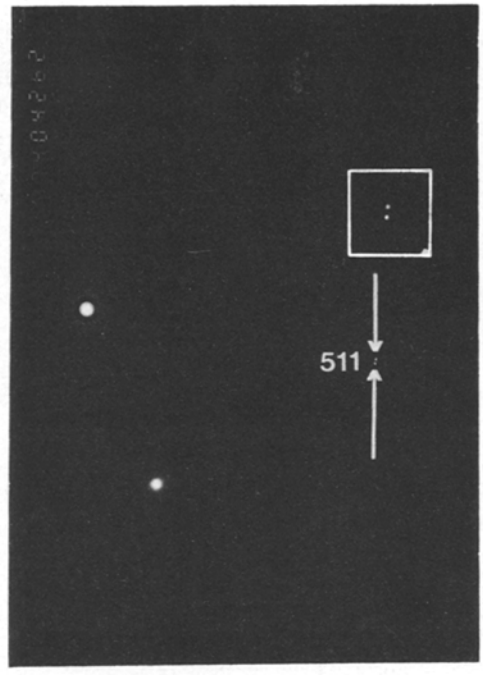

Figure 7 **Splitting of the 511 diffraction spot, showing the small-angle rotation. The inset corresponds to the duplicated 511 and is taken with a larger camera length. Encircled is the transmitted beam.**

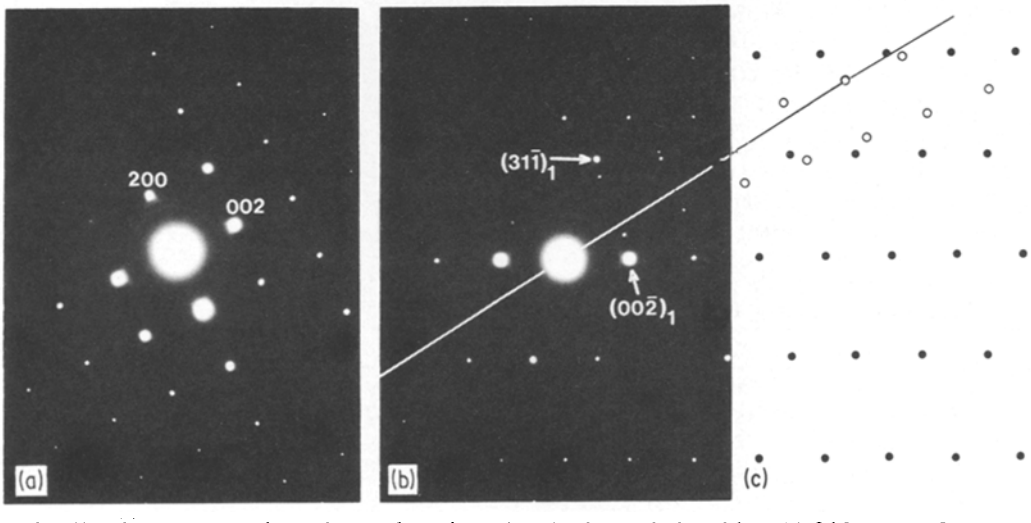

Figure 8 Diffraction patterns taken with the boundary plane in the vertical position. (a) 010 pattern from crystal 2, (b) diffraction pattern from both crystals and graphical extension where open circles represent spots from crystal 2 and black dots spots from crystal 1, which appear to be near to the $[1\bar{3}0]$ orientation.

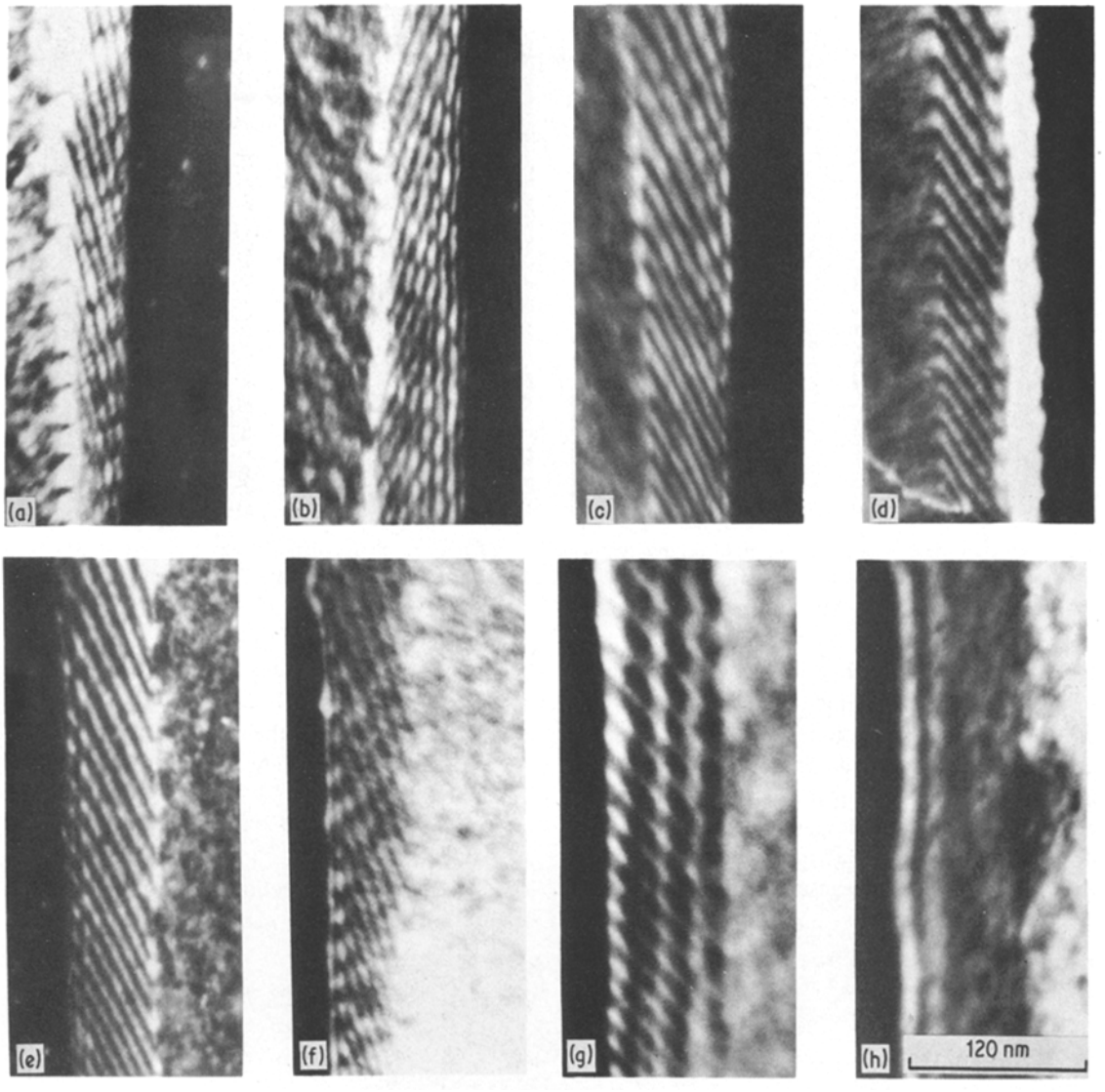

Figure 9 Dark-field images of the grain boundary and grain-boundary dislocations: (a) to (d) reflections from crystal 1, (a) $g = \bar{1}\bar{1}1$, (b) $g = 002$, (c) $g = 220$, (d) $g = \bar{1}\bar{1}3$; (e) to (h) reflections from crystal 2, (e) $g = \bar{1}1\bar{1}$, (f) $g = \bar{3}1\bar{1}$, (g) $g = 11\bar{3}$, (h) $g = 022$.

and b, crystal 1 is diffracting; in Fig. 10c and d, crystal 2 is diffracting. All the micrographs are taken with the electron beam close to the $[0\bar{1}1]$ direction, indicating a Burger's vector of the type $\boldsymbol{b} = [0\bar{1}1]$ and dislocations of pure edge character. Its length has not yet been determined.

Further confirmations are also given for common reflections in Fig. 11. The common $0\bar{2}2$ reflection is used in Fig. 11a, where the dislocations are in contrast. In Fig. 11b the common 511 reflection is used, where the dislocations are invisible and a Moiré-type contrast only is detected.

7. Discussion

The Burger's vectors for the DSC dislocations of a $\Sigma = 27a$ grain boundary are (see Appendix 2):

$$\frac{1}{27}[511], \frac{1}{27}[111\bar{6}] \text{ and } \frac{1}{27}[\bar{2}55].$$

Therefore, the $[0\bar{1}1]$ vector, possibly the $\frac{1}{2}[0\bar{1}1]$, is surprising. This may be formed by the following combination:

$$\frac{2}{27}[111\bar{6}] + \frac{1}{27}[\bar{2}55] \rightarrow [01\bar{1}]. \quad (17)$$

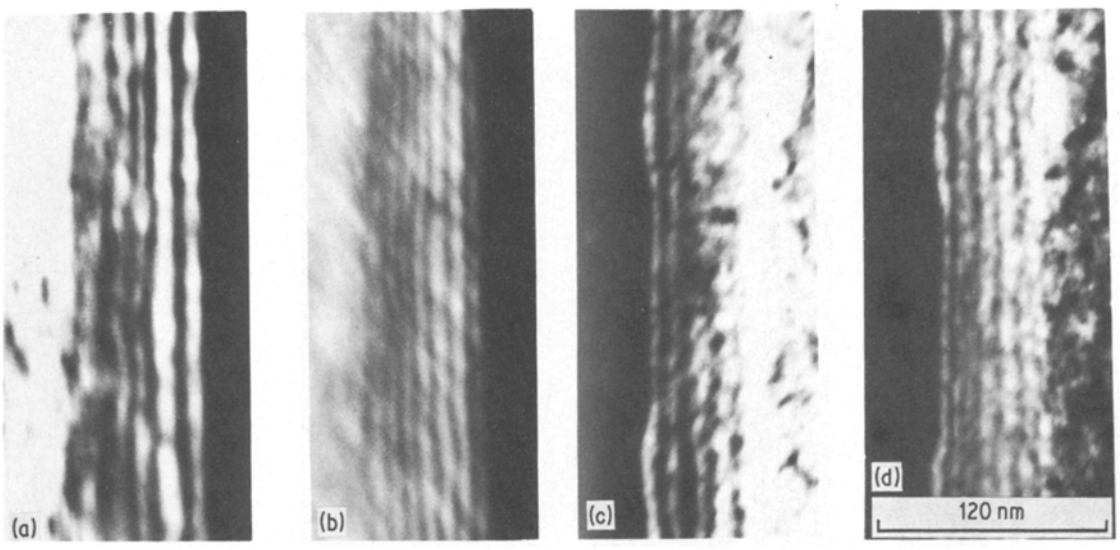

Figure 10 Dark-field images of the grain boundary formed by reflections of the planes of the common $[0\bar{1}1]$ zone axis. (a) $g = 200$, and (b) $g = \bar{1}11$ of crystal 1. (c) $g = \bar{1}11$, and (d) $g = 111$ of crystal 2. The invisibility criterion is valid for all these reflections.

It appears in this case that extrinsic secondary dislocations are not formed and that a preference for the primary dislocations, which are the matrix dislocations, is observed. These dislocations have, of course, a common Burger's vector in both crystal elements, since their Burger's vector is parallel to one of the 24 equivalent rotation axes describing the 27*a* CSL. It is suggested that this is not an isolated observation.

Fig. 12 presents a bright-field image of the boundary in a vertical orientation. Some dislocations are visible by the strain field they induce close to the surfaces. They also give rise to ledges in the boundary plane.

Appendix 1

The stereographic projection of the experimental orientation relationship can be constructed using

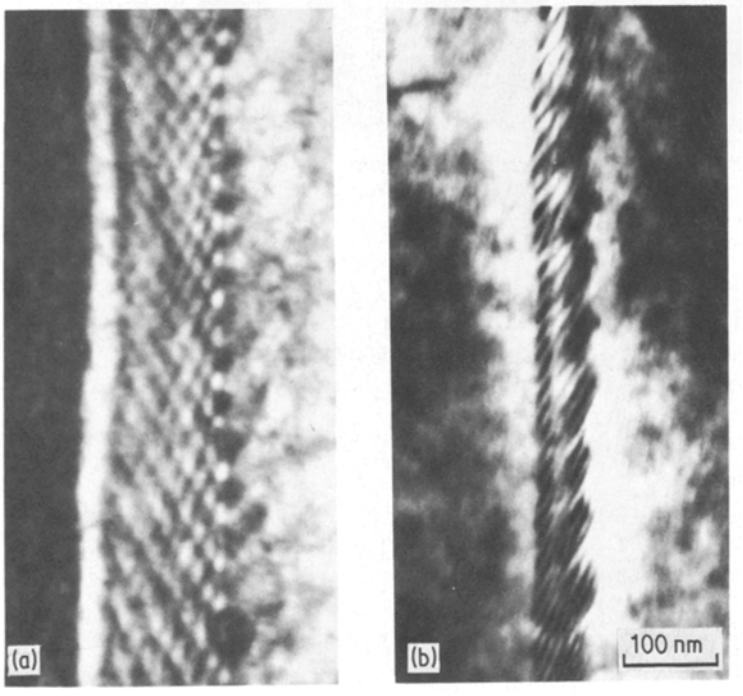

Figure 11 (a) Dark-field image using the common $0\bar{2}2$ reflection, grain-boundary dislocations and Moiré fringes are visible; (b) dark-field image using the common 511 reflection; only Moiré fringes are visible.

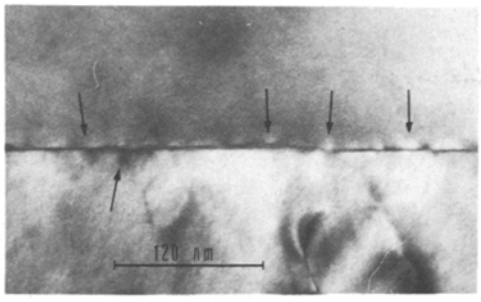

Figure 12 Stress-field contrast produced by the boundary dislocations.

the spherical co-ordinates of the 24 equivalent rotation axes taken from program GB1. This program gives also the co-ordinates of the crystallographic axes of the two grains. The projection is illustrated in Fig. A1, where the tilt axis is shown and the indices of the rotation axes are given in the system of grain 2. Since the orientation relationship of the two grains in this experiment corresponds almost to a perfect $\Sigma = 27a$ case the poles of the rotation axes in the projection in Fig. A1 are characterized by their ideal indices (see Tables I and II).

Appendix 2

The DSCL for the CSL $\Sigma = 27a$ has been computed using the modified 0-lattice [6].

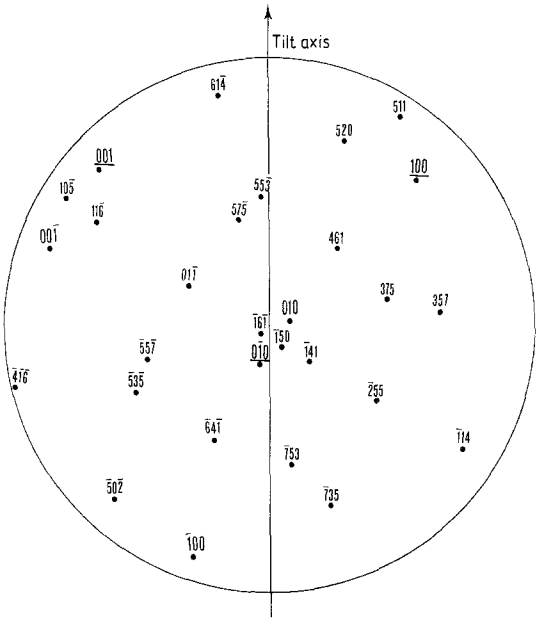

Figure A1 A stereographic projection of the bicrystal in the experimental position giving: the direction of the tilt axis; the crystallographic axes of grain 1 (100, 010, 001); the crystallographic axes of grain 2 (100, 010, 001) and the poles of the 24 equivalent rotation axes.

According to this, the rotation matrix Φ may be transformed using the following substitutions:

$$\alpha = \frac{u}{d^{1/2}}, \quad \beta = \frac{v}{d^{1/2}}, \quad \gamma = \frac{w}{d^{1/2}}, \tag{B1}$$

$$d = u^2 + v^2 + w^2, \tag{B2}$$

$$\cot\frac{\delta}{2} = \frac{m}{n d^{1/2}}, \tag{B3}$$

into the matrix

$$\Phi = \frac{1}{2nd}\begin{bmatrix} n(d+u^2) & uvn + wm & uwn - vm \\ uvn - wn & n(d+v^2) & vwn + um \\ uwn + vm & vwn - um & n(d+w^2) \end{bmatrix}, \tag{B4}$$

where:

$$\det \Phi = \frac{\alpha\Sigma}{4dn}, \tag{B5}$$

$$\sum = \frac{m^2 + dn^2}{\alpha}. \tag{B6}$$

Since we know that the CSL basis $[\mathbf{x}]_{CSL}$ may be found from the relation:

$$[\mathbf{x}]_{CSL} = \Phi\,[\mathbf{x}]_t, \tag{B7}$$

where $[\mathbf{x}]_t$ is the 3 x 3 matrix of the rotation axis vector and two t-vectors, the problem is the choice of the $[\mathbf{x}]_t$ matrix. We may easily see that:

$$\det[\mathbf{x}]_{CSL} = \det\Phi \cdot \det[\mathbf{x}]_t \tag{B8}$$

and since $\det[\mathbf{x}]_{CSL} = \Sigma$, Equations B5 and B8 imply:

$$\det[\mathbf{x}]_t = \frac{4dn^2}{\alpha}. \tag{B9}$$

In the present case the rotation axis is the [5 1 1] and the rotation angle 180°, that is:

$$m = 0,\ n = 1,\ \Sigma = 5^2 + 1^2 + 1^2 = 27$$
$$\text{and } \alpha = 1.$$

Therefore,

$$\det[\mathbf{x}]_t = 108. \tag{B10}$$

Thus, the determinant $\det[\mathbf{x}]_t$ gives:

$$5[v_1 w_2 - w_1 v_2] - [u_1 w_2 - u_2 w_1] + [u_1 v_2 - v_1 u_2] = 108, \tag{B11}$$

where $t_1 = (u_1 v_1 w_1)$, $t_2 = (u_2 v_2 w_2)$. By using

two more equations which are obvious from the t-lattice definition [6]:

$$\begin{aligned} 5u_1 + v_1 + w_2 &= 0 \\ 5u_2 + v_2 + w_2 &= 0 \end{aligned} \tag{B12}$$

we may have

$$\begin{aligned} t_1 &= (02\bar{2}) \\ t_2 &= (\bar{2}82). \end{aligned} \tag{B13}$$

Then Equation 7 may be expressed as:

$$\begin{bmatrix} 5 & 0 & \bar{1} \\ 1 & 1 & 4 \\ 1 & \bar{1} & 1 \end{bmatrix} = \frac{1}{54} \begin{bmatrix} 52 & 5 & 5 \\ 5 & 28 & 1 \\ 5 & 1 & 28 \end{bmatrix} \cdot \begin{bmatrix} 5 & 0 & \bar{2} \\ 1 & 2 & 8 \\ 1 & \bar{2} & 2 \end{bmatrix}$$

and by taking into account that the DSC Lattice for the cubic system is the reciprocal lattice of the CSL, the vectors

$$(5\,1\,1),\ (1\,11\,\bar{1}\bar{6}),\ (\bar{2}\,5\,5)$$

form a basis for the DSC lattice.

References

1. W. BOLLMANN, "Crystal Defects and Crystalline Interfaces" (Springer, Berlin, 1970).
2. P. H. PUMPHREY, "Grain Boundary Structure and Properties", edited by G. A. Chadwick and D. S. Smith (Academic Press, New York, 1976) p. 139.
3. D. H. WARRINGTON and H. GRIMMER, *Phil. Mag.* **30** (1974) 461.
4. L. PRIESTER, *Rev. Phys. Appl.* **15** (1980) 789.
5. TH. KARAKOSTAS, G. NOUET, G. L. BLERIS, S. HAGEGE and P. DELAVIGNETTE, *Phys. Stat. Sol. (a)* **50** (1980) 703.
6. TH. KARAKOSTAS, G. NOUET and P. DELAVIGNETTE, *ibid.* **52** (1979) 65.
7. TH. KARAKOSTAS, G. L. BLERIS and J. G. ANTONOPOULOS, *ibid.* **55** (1979) 801.
8. G. L. BLERIS, J. G. ANTONOPOULOS, TH. KARAKOSTAS and P. DELAVIGNETTE, *ibid.* **67** (1981) 249.
9. G. L. BLERIS, S. HAGEGE, G. NOUET, J. G. ANTONOPOULOS, TH. KARAKOSTAS and P. DELAVIGNETTE, Proceedings of the 7th Congress on Electron Microscopy, Vol. 1, "Physics" (7th European Congress on Electron Microscopy Foundation, Leiden, 1980) p. 250.
10. G. L. BLERIS, TH. KARAKOSTAS and J. G. ANTONOPOULOS, *Sci. Annals. Fac. Phys. Math. Univ. Thessaloniki* **19** (1979) 91.
11. G. L. BLERIS and P. DELAVIGNETTE, *Acta Cryst.* **A37** (1981) 779.
12. G. L. BLERIS, TH. KARAKOSTAS and P. DELAVIGNETTE, to be published.

Received 7 January
and accepted 26 May 1982